Neuroradiology (2023) 65:1555–1559
https://doi.org/10.1007/s00234-023-03147-4

SHORT REPORT

# Feasibility of percutaneous dural sac puncture via a posterior trans-sacral foraminal conduit approach: a CT morphometric analysis

Siddhant S. Dhawan[1] · Fabian N. Necker[2,3] · Tarik F. Massoud[4,5]

Received: 27 December 2022 / Accepted: 31 March 2023 / Published online: 6 April 2023


## Abstract

We assess the theoretical feasibility of percutaneous posterior sacral foramen (pSF) needle puncture of the sacral dural sac (DS) by studying the three-dimensional imaging anatomy of pSFs relative to the sacral canal (SC). On CT images of 40 healthy subjects, we retrospectively studied sacral alae passageways from SC to pSFs in all three planes to determine if an imaginary spinal needle could theoretically traverse S1 or S2 pSFs in a straight path toward DS. If not straight, we measured multiplane angulations and morphometrics of this route. We found no straight connections between S1 or S2 pSFs and SC. Instead, there were bilateral spatially complex dorsoventral M-shaped "foraminal conduits" (FCs; common, ventral, and dorsal) from SC to anterior SFs and pSFs that would prevent percutaneous straight needle puncture of the DS. This detailed knowledge of the sacral FCs will be useful for accurate imaging interpretation and interventional procedures on the sacrum.

**Keywords** Fluoroscopy · Sacrum · Spinal puncture · Tomography · X-ray computed

## Introduction

A standard interlaminar lumbar puncture may be difficult or impossible in some patients, even with image guidance [1, 2]. An alternative procedure might be to puncture the sacral dura sac (DS) through a percutaneous trans-posterior sacral foraminal (pSF) approach (Fig. 1A–D). Indeed, Sujay et al. [3] and Paria et al. [4] described successful subarachnoid space (SAS) injection of anesthetics through S1 and S2 pSFs.

However, the sacrum is anatomically complex, and, to our knowledge, the precise spatial morphology and morphometrics of pSFs relative to the central sacral canal (SC) and DS terminations have not been studied previously. Here, we provide the first detailed description of the three-dimensional (3-D) imaging anatomy and morphometric CT image analysis of sacral foramina (SFs) connections to the SC. We hypothesized that if a straight path exists between SC and S1 or S2 pSFs, this in principle could favor the likelihood of unhindered percutaneous passage of a trans-pSF spinal needle to successfully access the SAS. We find instead that there are bilateral circuitous sacral "foraminal conduits" (FCs) that link pSFs to SC.

## Method

To help us conceive the intricate sacral FC system connected to the SC, we first created image segmentations of these structures from open source images, which we then visualized in an interactive, semi-transparent 3-D rendering (selected images in Fig. 1E). For details of this volume rendering and its video presentation, see Online Resources 1 and 2, respectively.

✉ Tarik F. Massoud
tmassoud@stanford.edu

1 Department of Bioengineering, Stanford University Schools of Engineering and Medicine, Stanford, USA

2 Stanford IMMERS (Incubator for Medical Mixed and Extended Reality), Department of Radiology, Stanford University School of Medicine, Stanford, USA

3 Institute of Functional and Clinical Anatomy, Digital Anatomy Laboratory, Friedrich-Alexander-University Erlangen-Nürnberg (FAU), Erlangen, Germany

4 Division of Neuroimaging and Neurointervention, and Stanford Initiative for Multimodality Neuro-Imaging in Translational Anatomy Research (SIMITAR), Department of Radiology, Stanford University School of Medicine, Stanford, USA

5 Department of Radiology, Stanford University Center for Academic Medicine, Radiology, MC: 5659; 453 Quarry Road, Palo Alto, CA 94304, USA

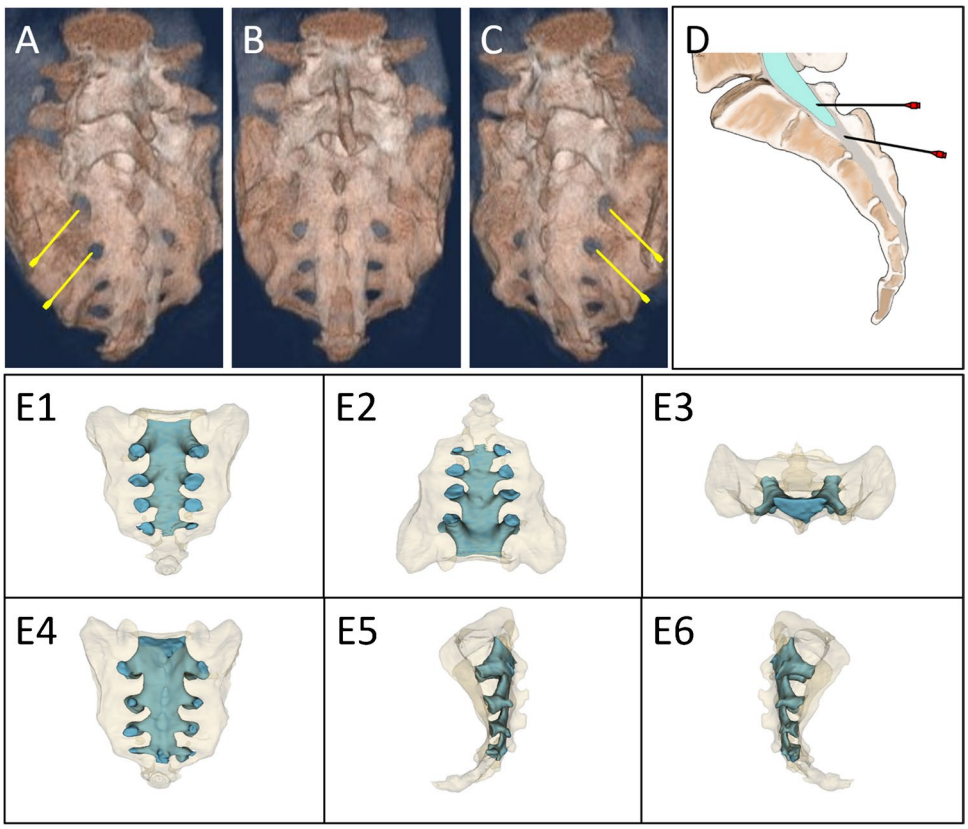


**Fig. 1** Illustrations of the concept for percutaneous trans-pSF puncture of the DS. Left oblique, frontal, and right oblique views (**A**–**C**) of hypothetical needles inserted in S1 and S2 pSFs of a sacrum created by 3-D volumetric reconstruction of contiguous 2 mm axial CT images in bone algorithm. A midsagittal schematic drawing of the sacrum and its DS shows positions of hypothetical needles obliquely inserted through S1 and S2 pSFs to target the SC and DS (**D**). 3-D anatomy of the complex sacral FCs connected to the SC shown in single images in different views (**E1**, anteroposterior; **E2**, cranio-caudal oblique; **E3**, cranio-caudal; **E4**, posteroanterior; **E5**, left lateral; and **E6**, right lateral) from a 3-D volume rendering video of these structures after post-processing and image segmentation of a sacrum CT scan (see Online Resource 1 for the methods used to produce this volume rendering and Online Resource 2 for its video presentation)

We obtained institutional ethical approval for this research study. We retrospectively selected 140 consecutive adult patients referred over a 2-year period for imaging of suspected CSF leaks using CT myelography, which has excellent high spatial resolution and separation of the DS from surrounding bones. Exclusion criteria for 100 patients were presence of transitional vertebrae (5), advanced degenerative changes (39), CSF leak positive (14), prior lumbosacral spine surgery (4), Tarlov cysts that might have remodeled adjacent bone (30), and connective tissue disorders potentially affecting the spine (8). An experienced neuroradiologist retrospectively analyzed all anonymized images of the remaining 40 patients with normal findings on a Sectra PACS workstation (Linköping, Sweden).

We first recorded patient age and sex distributions and calculated mean ages and standard deviations (SDs). On magnified midsagittal views of the distal spine, we recorded DS termination levels relative to the upper, mid, or lower parts of the adjacent sacral segments. We first digitally measured the midsagittal area ($mm^2$) of the SC. Next, we scrolled through the image stacks in all three planes to evaluate the passageways joining S1 and S2 pSFs to SC (see Online Resource 1 for details of measurements for widths and angles of these passageways). We calculated mean values and SDs for FC morphometrics and tested for statistical correlations, with significance set at $p < 0.05$.

## Results

Patient demographics are shown in Table 1. DS terminations were one at upper S1; one at mid S1; 14 at lower S1; two at upper S2; nine at mid S2; 11 at lower S2; one at upper S3; and one at lower S3.

None of the pSFs joined the SC along a straight path. Instead, there were bilaterally symmetrical, spatially complex 3-D shaped passageways that we termed FCs, consisting of common FC (CFC), ventral FC (VFC), and dorsal FC (DFC) leading from each central SC to bilateral anterior SFs (aSFs) and pSFs (Fig. 2A–E). When viewed axially,

**Table 1** Patient demographics, morphometrics, and statistical correlations for sagittal SC areas; axial DFC widths; and axial and coronal CFC-DFC angles at S1 and S2 in both sexes

| Characteristic | All subjects (mean ± SD) | Males $n=15$ (mean ± SD) | Females $n=25$ (mean ± SD) | † Statistical differences between males and females | ‡ Correlation of measurement with surface area of SC | ‡ Correlation of measurement with age |
|---|---|---|---|---|---|---|
| Age (years) | 44.9 ± 16.6 | 52.8 ± 16.7 | 40.2 ± 14.7 | N/A | N/A | N/A |
| Midsagittal cross-sectional area of SC | 727.1 ± 160.8 $mm^2$ | 899.7 ± 160.6 $mm^2$ | 698.3 ± 151.7 $mm^2$ | ***p* = 0.002** | N/A | $R^2=0.00$, $p=0.944$ |
| Width of the S1 DFC | 8.6 ± 1.6 mm | 8.2 ± 1.8 mm | 8.8 ± 1.5 mm | $p=0.29$ | $R^2=0.06$, $p=0.101$ | $R^2=0.05$, $p=0.150$ |
| Width of the S2 DFC | 6.7 ± 1.8 mm | 6.2 ± 2.0 mm | 7.1 ± 1.5 mm | $p=0.10$ | $R^2=0.028$, $p=0.296$ | $R^2=0.10$, ***p* = 0.044** |
| Axial plane CFC-DFC angle at S1 | 81.4° ± 5.7° | 79.5° ± 6.8° | 82.6° ± 4.8° | $p=0.11$ | $R^2=0.01$, $p=0.417$ | $R^2=0.01$, $p=0.400$ |
| Axial plane CFC-DFC angle at S2 | 88.7° ± 9.6° | 88.9° ± 11.5° | 88.6° ± 8.5° | $p=0.89$ | $R^2=0.200$, ***p* = 0.004** | $R^2=0.01$, $p=0.399$ |
| Coronal plane CFC-DFC angle at S1 | 89.1° ± 8.3° | 90.2° ± 9.3° | 81.3° ± 8.2° | $p=0.47$ | $R^2=0.099$, ***p* = 0.047** | $R^2=0$, $p=0.908$ |
| Coronal plane CFC-DFC angle at S2 | 80.8° ± 9.1° | 79.7° ± 10.7° | 81.4° ± 8.2° | $p=0.58$ | $R^2=0.01$, $p=0.494$ | $R^2=0.003$, $p=0.704$ |

†One-way analysis of variance (ANOVA) was used to determine statistical differences of measured characteristics between males and females

‡Linear regression was used to determine correlations of measurements with sacral canal surface area or age

Statistically significant if $p<0.05$. Significant correlations are in bold

*CFC*, common foraminal conduit; *DFC*, dorsal foraminal conduit; *N/A*, not applicable; *SC*, sacral canal; *SD*, standard deviation

rather than forming straight or mildly angled corridors from pSFs to SC, the FCs were bilateral symmetrically splayed M-shaped passageways (Fig. 2A–E). Each CFC bifurcated into a larger VFC leading ventrally to an aSF (as shown in Online Resource 1, Supplementary Figs. 1 and 2), and a smaller DFC leading dorsally (at an acute angle from the CFC bifurcation) to a pSF (see Fig. 2F and Online Resource 1 for further description of the 3-D spatial projections of these FCs). Morphometric results and statistical correlations are shown in Table 1.

## Discussion

We briefly review the intricate anatomy and embryology of the sacrum and its foramina in Online Resource 1. Whelan alluded to sacral internal anatomical complexity [5], and Jackson and Burke described Y-shaped complex sacral foraminal canals upon imaging of three dry sacra [6]. Hence, it was unclear to us if previously reported cases of trans-pSF punctures of the DS [3, 4] indicated a generalizable approach that could be more widely adopted based on anatomical feasibility. The pertinent question is whether the 3-D spatial anatomy of FCs would even permit a trans-pSF approach using a straight needle to puncture the DS.

Unlike our recently described percutaneous approach to the sacral DS via the sacral hiatus [7, 8], we found that absence of a straight path from S1 or S2 pSFs to SC would theoretically prohibit direct needle puncture of the DS in all 40 subjects. We observed that wider angles occur with larger SCs, likely because the latter splay the FC limbs further. We did not investigate S3 and S4 pSFs because of their considerable distance from DS terminations. The anatomical rationale for other percutaneous interventions via a trans-pSF approach is described in Online Resource 1.

We therefore speculate that reported seemingly successful trans-pSF needle punctures of the DS had possibly followed unwitting injection of Tarlov cysts close to pSFs (Online Resource 1, Supplementary Fig. 3) [9]. Selective needle targeting of the tiny CSF-filled S1 or S2 nerve perineural spaces would have been most unlikely, especially as sacral nerve roots have a long extradural course near foramina [10].

Study limitations include our small patient cohort, non-consideration of subtle changes in sacral morphology owing to normal variations, and non-measurement specifically of pSFs sizes, although we considered widths of S1 and S2 DFCs to be surrogate measurements for pSFs.

In conclusion, it would seem highly improbable or impossible that a straight spinal needle could reach the SC and penetrate the DS through a percutaneous pSF insertion at

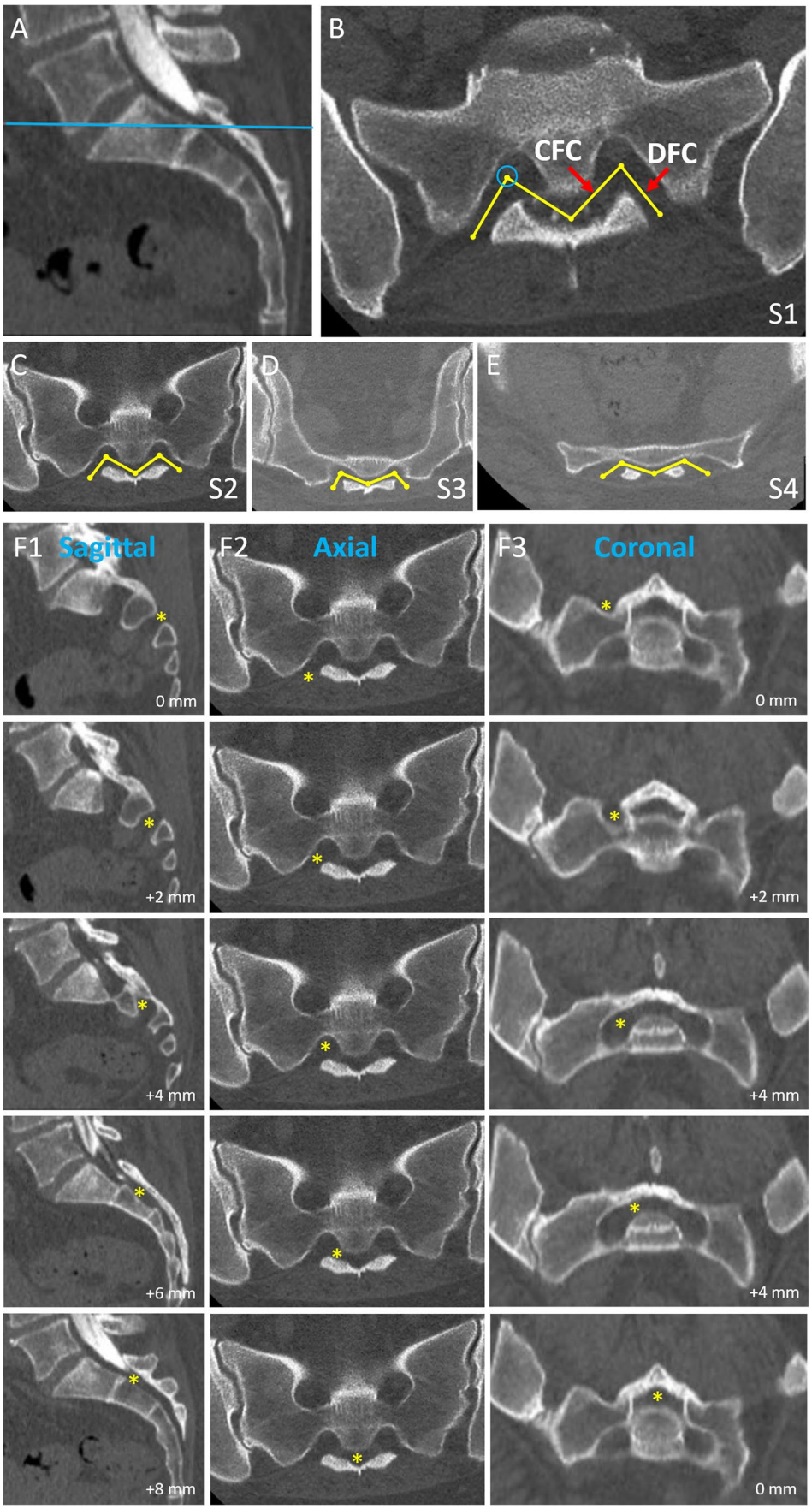


**Fig. 2** Spatial complexity of the FCs. Midsagittal image of CT myelogram shows reference line (blue) for S1 level axial image (**A**). Axial CT image at S1 shows bilaterally symmetrical FCs leading from each central SC to bilateral aSFs (not seen on this slice) and pSFs (**B**). A medially positioned CFC (arrow) and a more lateral DFC (arrow) leading to its pSF, along with contralateral FCs, are all laid out in the shape of a splayed "M" when viewing the sacrum in this supine position. Blue circle shows the CFC-DFC angle. Axial CT images show progressively greater splaying of the M-shaped FCs at S2 to S4, respectively (**C**–**E**). 3-D course of the right S2 DFC and CFC over 2-mm contiguous CT slices spanning the pSF to the SC (**F**), shown in orthogonal planes (**F1**–**F3**). S2 FCs are illustrated here on account of their shorter course than at S1. The changing asterisk positions mark the course of these FCs within the sacrum. Columns of sagittal (**F1**), axial (**F2**), and coronal images (**F3**) start at the right S2 pSF (asterisk in top images). All axial images are at the same slice, which shows that the course of M-shaped S2 FCs does not deviate to any large extent off a single axial plane. However, over a distance of 4 mm from the pSF, the DFC courses medially toward the midsagittal plane as well as a lower coronal plane to reach the CFC-DFC angle (middle row of images). Over another 4 mm from this angle, the CFC courses to the midsagittal plane as well as back to a higher coronal plane as it reaches the SC (lowest row of images)

S1 or S2 because of the complex 3-D spatial orientation of sacral FCs that we describe. Our characterization and new terminology for the sacral FCs will be useful for accurate diagnostic interpretation and to guide interventional sacral procedures.

**Supplementary information** The online version contains supplementary material available at https://doi.org/10.1007/s00234-023-03147-4.

**Acknowledgements** None.

**Author contributions** All authors contributed to the study conception and design. Material preparation, data collection, and analysis were performed by Siddhant S. Dhawan, Fabian N. Necker, and Tarik F. Massoud. The first draft of the manuscript was written by Siddhant S. Dhawan and Tarik F. Massoud and all authors commented on previous versions of the manuscript. All authors read and approved the final manuscript.

**Funding** The authors did not receive support from any organization for the submitted work. No funding was received to assist with the preparation of this manuscript. No funding was received for conducting this study. No funds, grants, or other support was received.

**Data Availability** Data generated or analyzed during the study are available from the corresponding author upon reasonable request.

## Declarations

**Ethics approval** We obtained ethical approval for this research study and waiver of individual patient consent from our local institutional review board administrative panel on human subjects in medical research. This approval was obtained from the ethics committee of Stanford University School of Medicine, USA (protocol: 55014). The procedures used in this study adhere to the tenets of the Declaration of Helsinki.

**Consent to participate and publish** This retrospective chart review study involving human participants was in accordance with the ethical standards of the institutional and national research.committee and with the 1964 Helsinki Declaration and its later amendments or comparable ethical standards. The Human Investigation Committee (IRB) of Stanford University School of Medicine, USA, approved this study (protocol: 55014). This included waiver of individual authorization for recruitment under title 45 CFR 164.512, pursuant to information provided in the HIPAA section of the protocol application. Consent was not required as patient information was anonymized and the publication submission does not include images that may identify the patient.

**Competing interests** The authors have no relevant financial or non-financial interests to disclose. The authors have no competing interests to declare that are relevant to the content of this article. All authors certify that they have no affiliations with or involvement in any organization or entity with any financial interest or non-financial interest in the subject matter or materials discussed in this manuscript. The authors have no financial or proprietary interests in any material discussed in this article.

## References

1. Hudgins PA, Fountain AJ, Chapman PR, Shah LM (2017) Difficult lumbar puncture: pitfalls and tips from the trenches. AJNR Am J Neuroradiol 38:1276–1283. https://doi.org/10.3174/ajnr.A5128
2. Nascene DR, Ozutemiz C, Estby H, McKinney AM, Rykken JB (2018) Transforaminal lumbar puncture: an alternative technique in patients with challenging access. AJNR Am J Neuroradiol 39:986–991. https://doi.org/10.3174/ajnr.A5596
3. Sujay M, Madhavi S, Aravind G, Hasan A, Venugopalan VM (2014) Transforaminal sacral approach for spinal anesthesia in orthopedic surgery: a novel approach. Anesth Essays Res 8:253–255. https://doi.org/10.4103/0259-1162.134526
4. Paria R, Surroy S, Majumder M, Paria B, Paria A, Das G (2014) Sacral spinal anaesthesia. Indian J Anaesth 58:80–82. https://doi.org/10.4103/0019-5049.126809
5. Whelan MA, Gold RP (1982) Computed tomography of the sacrum: 1. normal anatomy. AJR Am J Roentgenol 139:1183–1190. https://doi.org/10.2214/ajr.139.6.1183
6. Jackson H, Burke JT (1984) The sacral foramina. Skeletal Radiol 11:282–288. https://doi.org/10.1007/BF00351354
7. Trinh A, Hashmi SS, Massoud TF (2021) Imaging anatomy of the vertebral canal for trans-sacral hiatus puncture of the lumbar cistern. Clin Anat 34:348–356. https://doi.org/10.1002/ca.23612
8. Dhawan SS, Trinh A, Massoud TF (2023) Feasibility of intrathecal therapeutic injections in spinal muscular atrophy patients via a percutaneous transsacral hiatus route: an initial neuroimaging morphometric study. Muscle Nerve 67:226–230. https://doi.org/10.1002/mus.27782
9. Baker M, Wilson M, Wallach S (2018) Urogenital symptoms in women with Tarlov cysts. J Obstet Gynaecol Res 44:1817–1823. https://doi.org/10.1111/jog.13711
10. Liguoro D, Viejo-Fuertes D, Midy D, Guerin J (1999) The posterior sacral foramina: an anatomical study. J Anat 195:301–304. https://doi.org/10.1046/j.1469-7580.1999.19520301.x